Probing the semiconductor to semimetal transition in InAs/GaSb double quantum wells by magneto-infrared spectroscopy

Y. Jiang,[1] S. Thapa,[2] G. D. Sanders,[2] C. J. Stanton,[2] Q. Zhang,[3] J. Kono,[3] W. K. Lou,[4,5] K. Chang,[4,5] S. D. Hawkins,[6] J. F. Klem,[6] W. Pan,[6] D. Smirnov,[7] and Z. Jiang[1,*]

[1]*School of Physics, Georgia Institute of Technology, Atlanta, Georgia 30332, USA*

[2]*Department of Physics, University of Florida, Gainesville, Florida 32611, USA*

[3]*Department of Electrical and Computer Engineering, Department of Physics and Astronomy, and Department of Materials Science and NanoEngineering, Rice University, Houston, Texas 77005, USA*

[4]*SKLSM, Institute of Semiconductors, Chinese Academy of Sciences, Beijing 100083, China*

[5]*Synergetic Innovation Center of Quantum Information and Quantum Physics, University of Science and Technology of China, Hefei, Anhui 230026, China*

[6]*Sandia National Laboratories, Albuquerque, New Mexico 87185, USA*

[7]*National High Magnetic Field Laboratory, Tallahassee, Florida 32310, USA*

(Received 2 November 2016; published 11 January 2017)

We perform a magnetoinfrared spectroscopy study of the semiconductor to semimetal transition of InAs/GaSb double quantum wells from the normal to the inverted state. We show that owing to the low carrier density of our samples, the magnetoabsorption spectra evolve from a single cyclotron resonance peak in the normal state to multiple absorption peaks in the inverted state with distinct magnetic field dependence. Using an eight-band Pidgeon-Brown model, we explain all the major absorption peaks observed in our experiment. We demonstrate that the semiconductor to semimetal transition can be realized by manipulating the quantum confinement, the strain, and the magnetic field. Our work paves the way for band engineering of optimal InAs/GaSb structures for realizing novel topological states as well as for device applications in the terahertz regime.

DOI: 10.1103/PhysRevB.95.045116

I. INTRODUCTION

Broken-gap InAs/GaSb double quantum wells (DQWs) have long been important in studying intriguing phenomena, including excitonic resonances [1,2], electron-hole hybridization [3–6], the quantum spin Hall (QSH) effect [7–9], helical Luttinger liquids [10], and exciton insulators [11]. The novel properties of the InAs/GaSb system stem from its peculiar band-edge alignment, in which the bottom of the InAs conduction band lies below the top of the GaSb valence band [Fig. 1(a)], resulting in the separation of electrons and holes into the two QWs. By changing the width of each QW, one can manipulate the electron and hole energy levels using the quantum confinement effect. Specifically, when the lowest electron level E_0 in InAs lies above the highest hole level H_0 in GaSb, the system is in the normal state ($E_0 > H_0$). When the opposite alignment $E_0 < H_0$ is achieved, the system is said to be in the inverted state. The transition from normal to inverted states occurs at the critical QW widths at which $E_0 = H_0$ [Fig. 1(b)]. Recently, the QSH effect has been theoretically predicted [7] and experimentally explored [8,9] in the inverted regime, while an exciton-insulator-like state [11] and a giant supercurrent state [12] have been found in the vicinity of the critical state. Therefore, precise control of band alignment of InAs/GaSb DQWs from the normal to the inverted state is crucial for future fundamental studies. In particular, a thorough understanding of strain effects may lead to a robust QSH insulator state suited for realizing Majorana fermions [13].

From technological perspective, InAs/GaSb-based materials are promising candidates for third-generation infrared (IR) detectors [14], high-power light emitting diodes [15], and tunnel field-effect transistors [16], owing to their band engineering flexibility and the resulting low Auger recombination rates [17]. Practical applications of the material require a complete understanding of the electronic band structure, with respect to external parameters such as strain and doping. Previous combined experimental and theoretical studies [3–6] largely focused on the heavily inverted regime using reduced models. Quantitative investigations of the transition from the normal to the inverted state have not yet been performed.

In this paper, we study the evolution of the electronic band structure of InAs/GaSb DQWs across the semiconductor to semimetal transition using magneto-IR spectroscopy [18]. The observed magneto-optical modes can be explained using an eight-band $\mathbf{k}\cdot\mathbf{p}$ model, and semiquantitative agreement is achieved. We show that in addition to the commonly used electrostatic gate, the normal to the inverted state transition can be manipulated in a much larger parameter space via tuning the relative thickness of the QWs, the strain, and the magnetic field.

II. EXPERIMENT

The InAs/GaSb DQW samples studied in this work were grown by molecular beam epitaxy (MBE) on GaSb (001) substrates. A schematic of the epistructure is shown in Fig. 1(c), where the InAs/GaSb DQW structure is sandwiched between two AlSb barrier layers. To study the normal to inverted transition, we fabricated a series of five InAs/GaSb DQW samples. We fixed the width of the GaSb QW at 5 nm, while varying the InAs QW width from $d = 8$ to 10, 11, 13, and 15 nm. Based on our self-consistent eight-band $\mathbf{k}\cdot\mathbf{p}$ calculation (to be elaborated later), the $d = 8$-nm sample is in

*zhigang.jiang@physics.gatech.edu

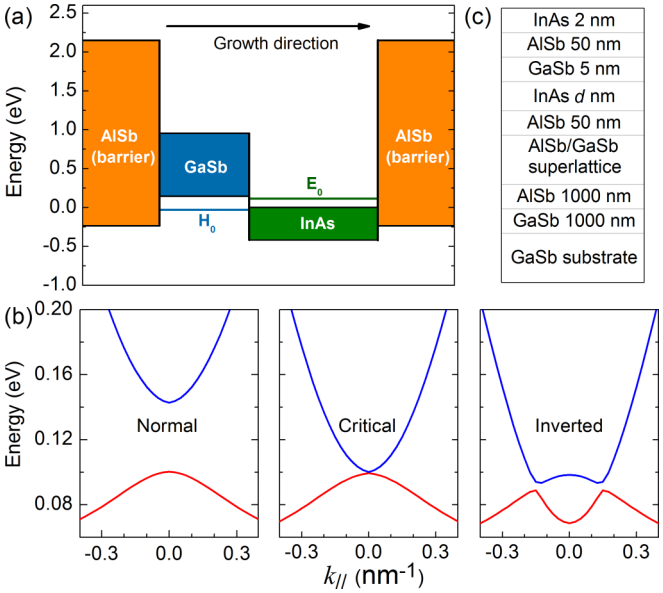

FIG. 1. (a) Schematic band diagram of AlSb/InAs/GaSb/AlSb QW structure. The energy zero is referenced to the conduction-band edge of bulk InAs. The top and bottom of each color coded blocks indicate the energies of the conduction- and valence-band edges for each material. E_0 and H_0 illustrate the lowest electron subband in InAs and the highest hole subband in GaSb, respectively, due to quantum confinement. (b) Evolution of the band alignment in InAs/GaSb DQWs, as the width d of the InAs QW increases (from left to right) while fixing the GaSb QW width. Blue and red curves represent the lowest electron and highest hole subbands, respectively. (c) Epistructure of MBE grown InAs/GaSb DQW samples.

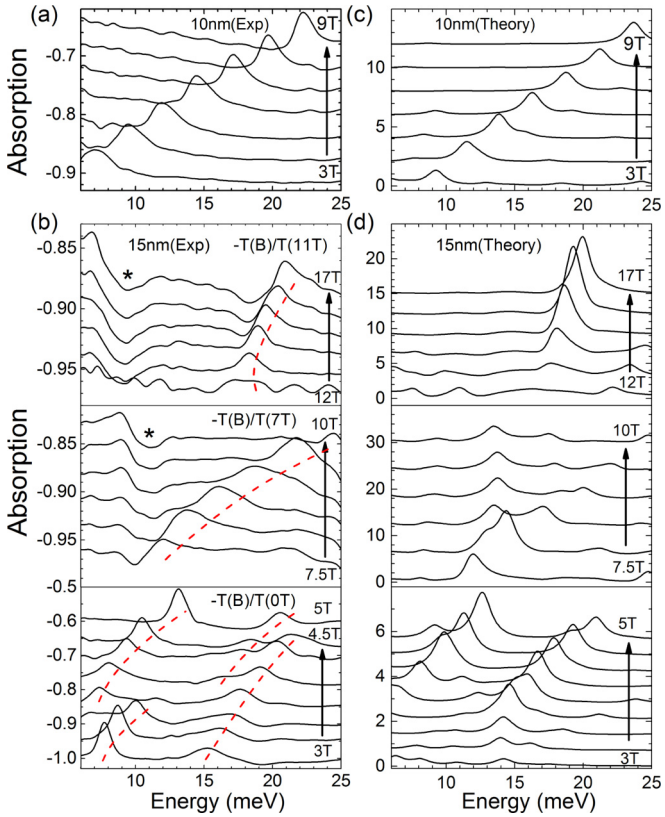

FIG. 2. (a) Normalized magnetoabsorption spectra, $-T(B)/T(B=0)$, for the slightly inverted InAs/GaSb DQW sample ($d = 10$ nm) at selected magnetic fields. (b) Normalized magnetoabsorption spectra for the heavily inverted sample ($d = 15$ nm) in the high-field (top panel), intermediate-field (middle panel), and low-field (bottom panel) regions. For best presentation, the spectra are normalized to 11, 7, and 0 T, respectively, for each panel. The star symbols point to B-independent spectral features originating from the normalization process. The dashed lines indicate the major absorption peaks observed in the experiment. (c,d) Calculated magnetoabsorption spectra using the eight-band PB model, in comparison with the experimental results in (a) and (b). In all panels, the spectra are offset vertically for clarity.

the normal state, the $d = 10$-nm sample is close to the critical state, and the $d = 11$-, 13-, and 15-nm samples are in the inverted state. Magnetotransport measurements determined the carrier densities to be as low as $n \sim 1 \times 10^{11}$ cm^{-2} [12], several times lower than that reported in previous studies [1–3,5,6]. Therefore, our samples are close to the dilute limit, particularly suited for magneto-optical spectroscopy studies.

Magneto-IR spectroscopy measurements were performed in the Faraday configuration at liquid helium temperature (4.2 K) using a Bruker 80v Fourier-transform IR spectrometer. The (unpolarized) IR radiation from a mercury lamp was delivered to the sample located at the center of a 17.5-T superconducting magnet via evacuated light pipes, and the intensity of the transmitted light was detected by a composite Si bolometer mounted beneath the sample. Normalized magnetoabsorption spectra were then obtained by taking the ratio of $-T(B)/T(B=0)$, where $T(B)$ is the transmission spectrum measured at a constant magnetic field B. In this scenario, the intraband (cyclotron resonance, CR) and interband Landau-level (LL) transitions are expected to manifest themselves as a series of absorption peaks.

Figure 2(a) shows normalized magnetoabsorption spectra, $-T(B)/T(B=0)$, for the $d = 10$-nm DQW sample at selected magnetic fields. Here, the spectra exhibit a single symmetric line, indicative of a single absorption peak within the energy range of our measurements. The spectral line shape becomes asymmetric and substantially broadened in the $d = 11$-nm sample, as shown in Fig. S1 in Ref. [20]. As the InAs QW width increases further to $d = 13$ nm (Fig. S2) and $d = 15$ nm [Fig. 2(b)], the InAs/GaSb DQWs enter a heavily inverted regime and multiple absorption peaks appear. Experimentally, one can identify four peaks for the case of $d = 15$ nm in Fig. 2(b) in the low-field region, $B \leqslant 5$ T. The two lower-energy peaks are CR-like, $E_{\mathrm{CR}} \propto B$, while the higher-energy ones can be attributed to interband LL transitions. Interestingly, the CR-like peaks deviate from their linear-in-B dependence at higher magnetic field [better seen in Fig. 4(d)], suggestive of LL crossing/anticrossing. This behavior is consistent with that theoretically predicted in Ref. [21]. In the middle and upper panels of Fig. 2(b), one can find another two absorption peaks with distinct B dependence. In particular, the high-field peak exhibits very weak B dependence, similar to that reported for InAs/GaSb superlattices in Ref. [3]. The observation of a total of six absorption peaks in the $d = 15$-nm DQW sample [Fig. 4(d)]

can be attributed to its low carrier density (approaching the dilute limit). However, the literature lacks a quantitative model that can interpret all these peaks.

III. THEORETICAL CALCULATION AND DISCUSSION

To explain how band inversion changes the LL transitions in InAs/GaSb DQWs, we employ an eight-band Pidgeon-Brown (PB) model [22] that includes the interaction between the conduction and valence bands, the Zeeman energy, and the effect of spin-orbit coupling. The PB model is based on an eight-band $\mathbf{k}\cdot\mathbf{p}$ method, described in the literature [21,23–27], which has been successfully used for achieving semiquantitative understanding of the electronic and magneto-optical properties of narrow-gap semiconductors [28–31]. We paid special attention to two important effects: (1) the effect of strain due to the lattice mismatch among different QW layers and (2) the effect of charge transfer through the InAs/GaSb interface. We assume that the system is under pseudomorphic strain and all the QW in-plane lattice constants are pinned to the in-plane lattice constant of the GaSb substrate. The strain gives rise to an energy shift of a few tens of meV and drives the system towards a more inverted band alignment. This effect is significant for all the DQW samples studied. The charge-transfer effect, on the other hand, is appreciable only in the inverted state [32] when the valence band of GaSb overlaps with the conduction band of InAs. This overlap leads to charge redistribution across the InAs/GaSb interface, which consequently modifies the potential profile in DQWs. The charge-transfer effect counters, or even overpowers, the strain effect in heavily inverted InAs/GaSb samples. It can be accommodated by solving the $\mathbf{k}\cdot\mathbf{p}$ equations iteratively until the potential profile reaches convergence. Further detailed information (including an improved self-consistent algorithm) can be found in Ref. [20].

In the presence of a magnetic field, the total effective mass Hamiltonian of InAs/GaSb DQWs can be written as

$$H = H_L + H_Z + H_S + H_C, \tag{1}$$

where H_L, H_Z, H_S, and H_C are the Landau, Zeeman, strain, and confinement Hamiltonian, respectively. Following the PB formalism, one can then solve the Schrödinger equation with a convenient set of envelope functions $F_{p,v}$ in the axial approximation,

$$H_p F_{p,v} = E_{p,v} F_{p,v}, \tag{2}$$

where the integer p is the PB manifold index and $p \geqslant -1$, and the integer v labels the eigenvectors and eigenenergies belonging to the same index p. We note that the Landau Hamiltonian H_L in Eq. (1) is p dependent, whereas H_Z, H_S, and H_C are independent of p. The explicit expressions of these terms are given in Refs. [28,29]. Next, the matrix eigenvalue equations of Eq. (2) can be solved separately for each allowed value of p and the eigenenergy $E_{p,v}$ is obtained as a function of magnetic field.

The calculated energy levels and Fermi energy E_F are plotted as a function of magnetic field in Figs. 3 and S3 for all the DQW samples studied. The PB manifold is color coded based on the index p, and for simplicity we only show the lowest levels, i.e., when $p = -1$, 0, 1, and 2. As one

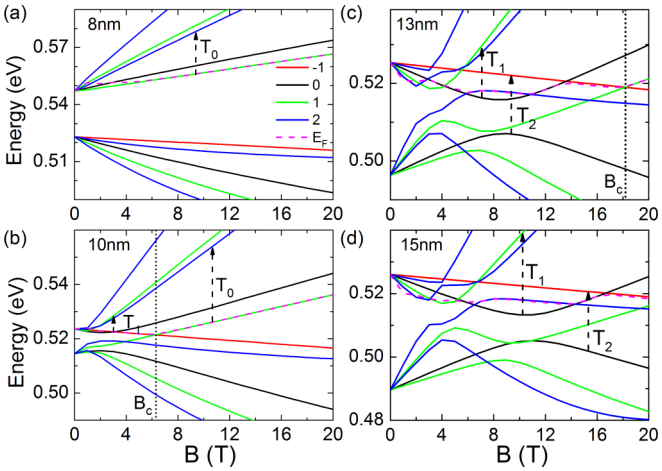

FIG. 3. Calculated energy levels as a function of magnetic field for (a) $d = 8$-, (b) 10-, (c) 13-, and (d) 15-nm InAs/GaSb DQW samples. The PB manifold is color coded based on the index p, and the dashed line shows the evolution of E_F as a function of magnetic field. The dashed arrows indicate the major transitions, T_0, T_1, and T_2, commonly observed in our samples. The dotted lines mark the onset (B_c) of the magnetic field driven transition from the inverted to the normal state.

can clearly see in Fig. 3, the band structure of InAs/GaSb DQWs exhibits a transition from the normal to the inverted state with increasing InAs QW width d. In the normal state [Fig. 3(a)], the electron (hole) levels reside in the conduction (valence) band and the energy of each level shows a monotonic B dependence without any crossing. In contrast, when the band is inverted [Figs. 3(b)–3(d)], holelike levels may exist at the bottom of the conduction band while electronlike levels appear at the top of the valence band. These levels inevitably cross or anticross each other at sufficiently high magnetic field, leading to multiple magnetoabsorption peaks. The magnitude of the crossing/anticrossing magnetic field therefore characterizes the degree of band inversion. One can see from Fig. 3 that the $d = 10$-nm DQW sample is only slightly inverted, whereas the $d = 13$- and 15-nm samples are heavily inverted. In addition, we note that even for a heavily inverted band structure, the electronlike levels in the valence band can be lifted above all the holelike levels, at sufficiently high magnetic fields, driving the system to the normal state [1,33–35]. We will return to this magnetic field driven semimetal to semiconductor transition in the context of Fig. 5.

In order to calculate the magneto-optical absorption spectra, we first determine E_F using a standard routine described in Ref. [28] assuming an electron density of $n = 0.9 \times 10^{11}$ cm^{-2}. Second, we compute the magnetoabsorption coefficient using the wave functions obtained from the PB model and Fermi's golden rule [28,29]. The full width at half maximum is taken to be 0.8 meV in our calculation, estimated from the experimental data. The deduced selection rule reads $\Delta p = \pm 1$, where $+$ $(-)$ denotes electronlike (holelike) transitions. Figures 2(c) and 2(d) show the calculated magnetoabsorption spectra for the slightly inverted ($d = 10$ nm) and heavily inverted ($d = 15$ nm) DQW samples, in comparison with the experimental data in Figs. 2(a) and

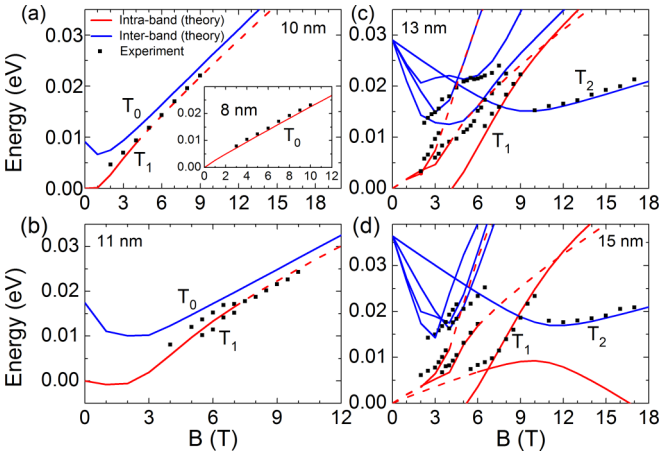

FIG. 4. Magnetic field dependence of major absorption peaks, both experimental and theoretical, for the $d = 8$- (inset to panel a), 10- (a), 11- (b), 13- (c), and 15-nm (d) DQW samples. The blue (red) solid lines represent the manifold-resolved interband (intraband) transitions. For simplicity, we only label the commonly observed transitions, T_0, T_1, and T_2, in our samples. Complete assignment of all transitions can be found in Table S2. The red dashed lines indicate the diminishing absorption peaks (Pauli) blocked when the corresponding level crosses above the Fermi energy.

2(b). The same normalization method is applied to both the experimental and theoretical results. Here, as one can see, the calculated spectra capture all the absorption peaks observed in the experiment, although the relative strength between these peaks does not exhibit a perfect match. Better understanding of the data can be attained using the manifold-resolved magnetoabsorption spectra, some examples of which are shown in Fig. S4. Manifold-resolved calculations help assign a specific transition to each absorption peak observed in our experiment. For example, the CR peak observed in the $d = 8$ sample can be attributed to the T_0 transition from a $p = 1$ level to a $p = 2$ level ($1 \rightarrow 2$), as illustrated in Fig. 3(a). The manifold-resolved results are summarized in Fig. 4, where intraband (interband) transitions are color coded in red (blue). Semiquantitative agreement between the theory and experiment is reached [36].

It is important to note that our eight-band PB calculation is based on the band parameters reported in Ref. [37] with only two adjustable variables. One is the carrier density (or Fermi energy), which is set to be $n = 0.9 \times 10^{11}$ cm^{-2} for all the samples. As our DQWs are close to the dilute limit, the Fermi energy is expected to be quickly pinned to the lowest electron level with increasing magnetic field. The fact that only one absorption peak (T_0) is observed in the normal state ($d = 8$ nm) and slightly inverted ($d = 10$ nm) samples suggests an upper bound for the electron density, $n \leqslant 0.9 \times 10^{11}$ cm^{-2}. The slight broadening of the CR linewidth in the $d = 10$-nm sample at $B \leqslant 3$ T is indicative of the presence of the T_1 transition [Fig. 3(b)], which sets the lower bound for n. Therefore, one can conclude that $n = 0.9 \times 10^{11}$ cm^{-2} is a good approximation. The other variable used in our calculation is the effective mass of electrons in InAs QWs, which is determined experimentally as $m_e^* = 0.024 m_0$ by fitting to the CR (T_0) peak in the normal state ($d = 8$ nm) sample. Here, m_0 is the bare electron mass. In the inverted state, the contribution of m_e^* to the band structure is coupled to that of the charge-transfer effect discussed above. Therefore, m_e^* can only be extracted accurately from the normal state data.

In addition to the T_0 transition, it is intriguing to investigate the T_1 (intraband, $p : 0 \rightarrow 1$) and T_2 (interband, $p : 0 \rightarrow -1$) transitions denoted in Figs. 3 and 4. We note that in the normal state, T_1 is indiscernible from the T_0 transition. It starts to depart from T_0 when the band is slightly inverted [Figs. 4(a) and 4(b)], therefore it is responsible for the asymmetric line shape observed in the $d = 11$-nm sample (Fig. S1). As the band is further inverted, T_1 becomes a well-developed peak [Figs. 4(c) and 4(d)], but only occurs when the magnetic field lifts the $p = 1$ level (green) above the $p = 0$ level (black), as shown in Figs. 3(c) and 3(d). Therefore, T_1 can be used as an effective band-inversion indicator, and practically one can perform a linear-in-B fit to its energy at relatively high magnetic field, with the fitting intercept $y_0 \approx 0$ for the normal state, $y_0 < 0$ for the inverted state, and more negative value being more inverted. On the other hand, the T_2 transition only occurs in the inverted state and in the high-field region. It exhibits very weak B dependence, distinct from all the other absorption peaks we have observed. We attribute this peak to a holelike interband transition, $p : 0 \rightarrow -1$, due to the uplift of the heavy hole $p = -1$ level to the conduction band (i.e., band inversion). This observation is consistent with that reported in Ref. [3].

Lastly, we return to the magnetic field driven semimetal to semiconductor transition from the inverted to the normal state. As mentioned above, the heavy hole level ($p = -1$), inverted to the conduction band, would eventually cross below the lowest electron level ($p = 1$) with increasing magnetic field, driving the system back to the normal state. A critical field B_c can be defined at this crossing point [Figs. 3(b) and 3(c)], and the corresponding transition diagram is plotted in Fig. 5. The importance of the strain effect can also be seen in Fig. 5, as it significantly shifts the boundary between the inverted state and the magnetic field driven normal state. Practically, the strain effect can be engineered by choosing the appropriate substrate (typically, GaSb for pseudomorphic growth, GaAs for metamorphic growth) and the epistructure [13].

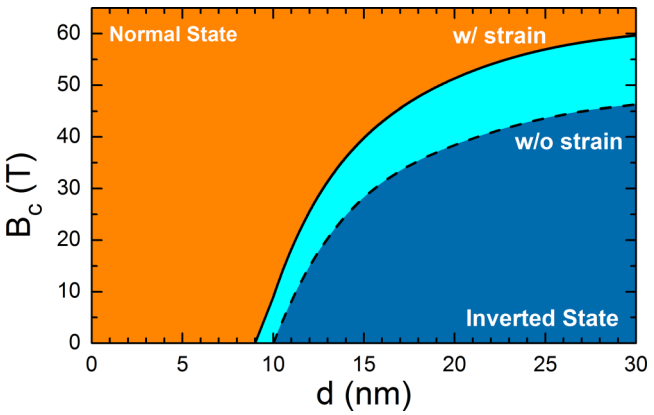

FIG. 5. Diagram describing the magnetic field driven semimetal to semiconductor transition from the inverted to the normal state, with and without strain. The width of GaSb QW is fixed to 5 nm. For demonstration purpose only, we omit the lengthy self-consistency calculation in this diagram.

IV. CONCLUSIONS

In conclusion, we have studied the LL structure of a series of InAs/GaSb DQWs from the normal to the inverted state using magneto-IR spectroscopy. We find that close to the dilute limit, the band inversion significantly modifies the magnetoabsorption of the system, giving rise to multiple absorption peaks with distinct nonlinear B dependence. All the major absorption peaks observed in our experiment can successfully be explained using an eight-band PB model, with semiquantitative agreement surpassing the previous two-band and eight-band models [3,6].

ACKNOWLEDGMENTS

We thank Danhong Huang for helpful discussion. This work was primarily supported by the U.S. Department of Energy (DOE) (Grant No. DE-FG02-07ER46451). S.T., G.D.S., and C.J.S. acknowledge support from the NSF (Grant No. DMR-1311849) and the AFOSR (Grant No. FA9550-14-1-0376). Q.Z. and J.K. acknowledge support from the NSF (Grant No. DMR-1310138). Z.J. acknowledges support from the National High Magnetic Field Laboratory (NHMFL), Visiting Scientist Program. The work at Sandia National Laboratories is supported by the DOE Office of Basic Energy Sciences, Division of Materials Science and Engineering, and by Sandia Laboratory Directed Research & Development (LDRD). Sandia National Laboratories is a multiprogram laboratory managed and operated by Sandia Corporation, a wholly owned subsidiary of Lockheed Martin Corporation, for the DOE's National Nuclear Security Administration under Contract No. DE-AC04-94AL85000. The magneto-IR measurements were performed at the NHMFL, which is supported by the NSF Cooperative Agreement No. DMR-1157490 and the State of Florida.

[1] J. Kono, B. D. McCombe, J. P. Cheng, I. Lo, W. C. Mitchel, and C. E. Stutz, Phys. Rev. B **50**, 12242(R) (1994); **55**, 1617 (1997); J. P. Cheng, J. Kono, B. D. McCombe, I. Lo, W. C. Mitchel, and C. E. Stutz, Phys. Rev. Lett. **74**, 450 (1995).

[2] L.-C. Tung, P. A. Folkes, G. Gumbs, W. Xu, and Y.-J. Wang, Phys. Rev. B **82**, 115305 (2010).

[3] G. M. Sundaram, R. J. Warburton, R. J. Nicholas, G. M. Summers, N. J. Mason, and P. J. Walker, Semicond. Sci. Technol. **7**, 985 (1992).

[4] M. J. Yang, C. H. Yang, B. R. Bennett, and B. V. Shanabrook, Phys. Rev. Lett. **78**, 4613 (1997).

[5] T. P. Marlow, L. J. Cooper, D. D. Arnone, N. K. Patel, D. M. Whittaker, E. H. Linfield, D. A. Ritchie, and M. Pepper, Phys. Rev. Lett. **82**, 2362 (1999).

[6] C. Petchsingh, R. J. Nicholas, K. Takashina, N. J. Mason, and J. Zeman, Physica E **12**, 289 (2002); Phys. Rev. B **70**, 155306 (2004).

[7] C. Liu, T. L. Hughes, X. L. Qi, K. Wang, and S. C. Zhang, Phys. Rev. Lett. **100**, 236601 (2008).

[8] I. Knez, R. R. Du, and G. Sullivan, Phys. Rev. Lett. **107**, 136603 (2011); L. Du, I. Knez, G. Sullivan, and R. R. Du, *ibid.* **114**, 096802 (2015).

[9] S. Mueller, A. N. Pal, M. Karalic, T. Tschirky, C. Charpentier, W. Wegscheider, K. Ensslin, and T. Ihn, Phys. Rev. B **92**, 081303(R) (2015).

[10] T. Li, P. Wang, H. Fu, L. Du, K. A. Schreiber, X. Mu, X. Liu, G. Sullivan, G. A. Csáthy, X. Lin, and R. R. Du, Phys. Rev. Lett. **115**, 136804 (2015).

[11] L. Du, W. Lou, K. Chang, G. Sullivan, and R.-R. Du, arXiv:1508.04509.

[12] X. Shi, W. Yu, Z. Jiang, B. A. Bernevig, W. Pan, S. D. Hawkins, and J. F. Klem, J. Appl. Phys. **118**, 133905 (2015).

[13] L. Du, T. Li, W. Lou, X. Wu, X. Liu, Z. Han, C. Zhang, G. Sullivan, A. Ikhlassi, K. Chang, and R.-R. Du, arXiv:1608.06588.

[14] A. Rogalski and P. Martyniuk, Infrared Phys. Technol. **48**, 39 (2006).

[15] L. M. Murray, D. T. Norton, J. T. Olesberg, T. F. Boggess, and J. P. Prineas, J. Vac. Sci. Technol. B **30**, 021203 (2012).

[16] J.-S. Liu, Y. Zhu, P. S. Goley, and M. K. Hudait, ACS Appl. Mater. Interfaces **7**, 2512 (2015).

[17] E. R. Youngdale, J. R. Meyer, C. A. Hoffman, F. J. Bartoli, C. H. Grein, P. M. Young, H. Ehrenreich, R. H. Miles, and D. H. Chow, Appl. Phys. Lett. **64**, 3160 (1994).

[18] Compared with magnetotransport methods, which could be dominated by chemically contaminated edge states [19], our magneto-IR technique is *bulk sensitive* and directly accesses the intrinsic properties of the material.

[19] F. Nichele *et al.*, New J. Phys. **18**, 083005 (2016).

[20] See Supplemental Material at http://link.aps.org/supplemental/10.1103/PhysRevB.95.045116 for additional experimental results and detailed information about the eight-band PB calculation.

[21] K. Nilsson, A. Zakharova, I. Lapushkin, S. T. Yen, and K. A. Chao, Phys. Rev. B **74**, 075308 (2006).

[22] C. R. Pidgeon and R. N. Brown, Phys. Rev. **146**, 575 (1966).

[23] A. Zakharova, S. T. Yen, and K. A. Chao, Phys. Rev. B **69**, 115319 (2004).

[24] I. Lapushkin, A. Zakharova, S. T. Yen, and K. A. Chao, J. Phys. Condens. Matter **16**, 4677 (2004).

[25] J. Li, K. Chang, G. Q. Hai, and K. S. Chan, Appl. Phys. Lett. **92**, 152107 (2008).

[26] J. Li, W. Yang, and K. Chang, Phys. Rev. B **80**, 035303 (2009).

[27] L.-H. Hu, C.-X. Liu, D.-H. Xu, F.-C. Zhang, and Y. Zhou, Phys. Rev. B **94**, 045317 (2016).

[28] G. D. Sanders, Y. Sun, F. V. Kyrychenko, C. J. Stanton, G. A. Khodaparast, M. A. Zudov, J. Kono, Y. H. Matsuda, N. Miura, and H. Munekata, Phys. Rev. B **68**, 165205 (2003).

[29] R. M. Wood, D. Saha, L. A. McCarthy, J. T. Tokarski, III, G. D. Sanders, P. L. Kuhns, S. A. McGill, A. P. Reyes, J. L. Reno, C. J. Stanton, and C. R. Bowers, Phys. Rev. B **90**, 155317 (2014).

[30] T. Kasturiarachchi, D. Saha, X. Pan, G. D. Sanders, M. Edirisooriya, T. D. Mishima, R. E. Doezema, C. J. Stanton, and M. B. Santos, J. Appl. Phys. **117**, 213914 (2015).

[31] E. G. Novik, A. Pfeuffer-Jeschke, T. Jungwirth, V. Latussek, C. R. Becker, G. Landwehr, H. Buhmann, and L. W. Molenkamp, Phys. Rev. B **72**, 035321 (2005).

[32] L. L. Chang, N. Kawai, G. A. Sai-Halasz, R. Ludeke, and L. Esaki, Appl. Phys. Lett. **35**, 939 (1979).
[33] I. V. Lerner and Y. E. Lozovik, J. Phys. C **12**, L501 (1979).
[34] D. J. Barnes, R. J. Nicholas, R. J. Warburton, N. J. Mason, P. J. Walker, and N. Miura, Phys. Rev. B **49**, 10474 (1994).
[35] M. A. Zudov, J. Kono, T. Ikaida, Y. H. Matsuda, N. Miura, S. Sasa, and M. Inoue, in *Proceedings of the 25th International Conference on the Physics of Semiconductors*, edited by N. Miura and T. Ando (Springer-Verlag, Berlin, 2001), p. 991.
[36] We stress that the semiquantitative agreement is reached by using one set of parameters for five InAs/GaSb DQW samples across the normal and inverted states.
[37] I. Vurgaftman, J. R. Meyer, and L. R. Ram-Mohan, J. Appl. Phys. **89**, 5815 (2001).